Available online at www.sciencedirect.com
SCIENCE DIRECT®
Chemical Physics Letters 376 (2003) 457–464
CHEMICAL PHYSICS LETTERS
www.elsevier.com/locate/cplett

Changes of the electronic structure along the internuclear coordinate studied by ultrafast photoelectron spectroscopy: the $2^1\Sigma_u^+$ Na_2 double-minimum state

M. Wollenhaupt, A. Assion, O. Graefe, D. Liese, C. Sarpe-Tudoran, M. Winter, T. Baumert *

Institute of Physics and Center for Interdisciplinary Nanostructure Science and Technology (CINSaT), University of Kassel, Heinrich-Plett-Str. 40, Kassel D-34132, Germany

Received 21 May 2003
Published online: 9 July 2003

Abstract

In a two-color femtosecond pump–probe experiment photoelectron spectra were detected to map the nuclear wave packet in the $2^1\Sigma_u^+$ Na_2 double-minimum state. The wave packet serves as a local probe for the R-dependent ionization probability. The pump photon energy of 3.65 eV allows to access a range of internuclear distances from 3 to 9 Å. The bound $1^2\Sigma_g^+$ and the repulsive $1^2\Sigma_u^+$ ionic states are accessible with the probe photon energy of 4.68 eV. Energy-resolved photoelectron measurements permitted to rule out competing ionization pathways. Our results show that for the bound ionic state the ionization probability at the outer turning point is 4.0 ± 0.4 times larger than that at the inner turning point.

1. Introduction

Femtosecond time-resolved multi-photon ionization is a widely spread technique to probe ultrafast atomic and molecular dynamics. The knowledge of the R-dependence of the transition dipole-moment for a neutral-to-ionic transition $\mu(R)$ is crucial for the interpretation of such pump–probe experiments. In theoretical descriptions of time-resolved photoelectron experiments the ionization probability is usually treated R-independently. However, if the probed state is characterized by more than a single diabatic contribution – leading to changes of the electronic structure along the internuclear coordinate – this approach seems to be no longer appropriate. The studies of Zewail and co-workers [1] on NaI highlight the role of R-dependent processes at avoided potential crossings. Moreover, the influence of the dipole functions $\mu(R)$ on the ultrafast photoionization of the Li_2 $^1\Sigma_u^+$ shelf state was carefully studied [2]. In polyatomic systems

* Corresponding author. Fax: +49-561-804-4453.
E-mail address: baumert@physik.uni-kassel.de (T. Baumert).

0009-2614/03/$ - see front matter
doi:10.1016/S0009-2614(03)00994-1

the role of excited state non-adiabatic effects on the ionization probability was investigated [3]. Moreover, a change of the electronic structure was also recognized to be an additional parameter in quantum control experiments [4].

Two-color pump–probe measurements on the NaI A state [5] employing photoion and photoelectron detection showed a change of the ionization cross section along the internuclear coordinate such that ionization only occurs in the ionic region of the A state. In a subsequent experiment using a resonant probe step at intermediate internuclear separation [6], the authors concluded a variation of the transition dipole moment of the resonant intermediate C state. An R-dependent transition dipole-moment for a neutral-to-ionic transition $\mu(R)$ has been investigated in other systems such as K_2, NaK and Na_2 as well using ion detection. Schwoerer et al. [7] studied the wave packet dynamics in the K_2 $B^1\Pi_u^+$ state. They could account for the experimental results by assuming a linear increase of $\mu(R)$ with bond length and an additional ionization pathway via autoionizing Rydberg states. The influence of different ionization pathways was studied in a one-color experiment on K_2 ionization via the K_2 $A^1\Sigma_u^+$ and K_2 $2^1\Pi_g$ states [8]. A higher ionization probability at larger internuclear distances was reported. However, this interpretation was compromised by the authors since interferences with doubly excited neutral states could not be ruled out. A decrease of $\mu(R)$ with increasing internuclear separation was observed in a one-color pump–probe experiment on the wave packet dynamics on the NaK $C^1\Sigma^+$ state [9]. Since ion detection was used the authors could not rule out other ionization pathways such as autoionizing neutral states.

As the Na_2 double-minimum state arises from an avoided crossing of diabatic states [10], the electronic structure changes rapidly along the internuclear coordinate. Therefore an R-dependent ionization probability is expected. For a general review see, for example, [11]. Indeed, a strong variation of $\mu(R)$ was theoretically predicted for the Na_2 double-minimum state [12–15]. For ionization at 544 nm negligible ionization was predicted for the inner potential well whereas an oscillating dipole moment was calculated for the barrier and the outer well [12]. In a two-color 340 nm pump and 540 nm probe experiment ions from the outer turning point were detected to obtain spectroscopic information of the Na_2 double-minimum state [16]. Using kinetic energy time-of-flight mass spectroscopy in a one-color (341.5 nm) pump–probe scheme [17] the dynamics of the wave packet on the Na_2 double-minimum state was mapped. In that experiment the repulsive ionic $1^2\Sigma_u^+$ state was not energetically accessible from the complete inner well and therefore the ionization probability could not be measured for all internuclear separations sampled by the wave packet. Applying time-resolved photoelectron detection in another one-color (340 nm) pump–probe experiment, the bound ionic $1^2\Sigma_g^+$ state was used to monitor the wave packet dynamics over the whole range of possible internuclear distances [4]. Analysis of the data in frequency domain has shown that the ionization at the outer turning point is favored but no direct comparison with time domain simulations was performed. Theoretical wave packet studies on this state employing an R-independent ionization probability [18] and focussing on effects of excitation/ionization with chirped femtosecond laser pulses [19,20] were reported in addition.

Here we report on a two-color ($\lambda_1 = 340$ nm) pump and ($\lambda_2 = 265$ nm) probe experiment (see Fig. 1) which is specifically designed to circumvent the above-mentioned restrictions through the choice of the appropriate probe wavelength and the use of time-resolved photoelectron detection. At an excitation wavelength of 340 nm, the generated wave packet oscillates between 3 and 9 Å and thus samples the inner Rydberg region and the outer well which has ionic character at large internuclear distances [12]. The ionization probe wavelength of 265 nm was chosen (i) to map the complete energetically allowed range of internuclear distances and (ii) to simultaneously project the wave packet motion on the $1^2\Sigma_g^+$ bound and the $1^2\Sigma_u^+$ repulsive ionic state. Since the photoelectron spectra directly reveal the ionization pathway competing ionization processes can be identified or ruled out [21,22]. More sophisticated information about the time evolution of the molecular electronic structure could be obtained with the use of angle-resolved photoelectron spectroscopy in principle as was studied theoretically [13,23] and also demonstrated

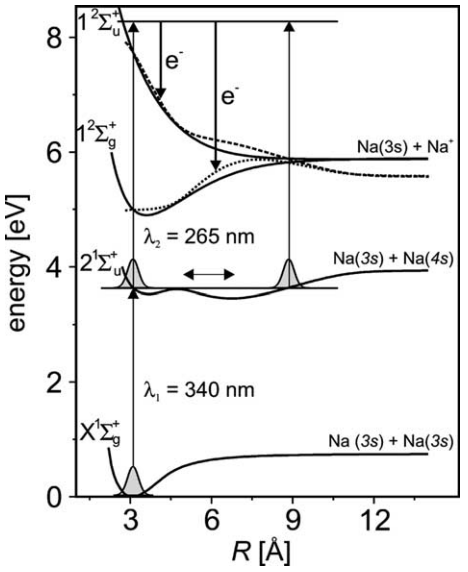

Fig. 1. Potential energy curves for $\lambda_1 = 340$ nm excitation of the $2^1\Sigma_u^+$ double-minimum state (pump) and subsequent $\lambda_2 = 265$ nm ionization to the bound $1^2\Sigma_g^+$ and repulsive $1^2\Sigma_u^+$ ionic states (probe). The corresponding difference potentials for the bound (dotted) and the repulsive (dashed) ionic states are displayed. Energy-resolved photoelectron spectra from both ionic states are measured.

experimentally [24,25]. The concept of our experiment is based on a direct comparison of measured angle-averaged pump–probe photoelectron spectra with simulations assuming an R-dependent ionization probability.

2. Theory

For comparison with the experiment we performed quantum mechanical simulations of the wave packet dynamics on the $2^1\Sigma_u^+$ double-minimum state using the experimental laser parameters, i.e., $\lambda = 340$ nm, 30 fs FWHM pulsed laser excitation and subsequent $\lambda_2 = 265$ nm, 40 fs FWHM ionization. Upon absorption of a 340 nm pump photon at the equilibrium internuclear distance of the $X^1\Sigma_g^+$ ($v'' = 0$) ground state at 3.1 Å, a wave packet is created at the inner turning point of the $2^1\Sigma_u^+$ double-minimum potential (see Fig. 1 for the relevant potential curves). The pump wavelength was chosen so that the energy of the wave packet slightly exceeds the barrier height and therefore samples a range of internuclear distances from 3 to 9 Å. The temporal evolution of the wave packet is depicted in Fig. 2.

Due to the anharmonicity of the double-minimum potential and the large number of coupled states (13 vibrational states within the FWHM of the pump spectrum), the wave packet dephases during the first couple of oscillations. Reflections at the barrier contribute negligibly to the wave packet dynamics at this excitation wavelength. However, the wave packet piles up at the inner edge of the barrier at 4.7 Å. The oscillation period is about 1 ps corresponding to the vibrational level spacing of approximately 32 cm^{-1} at $v' = 45$ (term energies taken from [26] and our calculations). The recurring wave packet shows spacetime interference structures as discussed in [27]. The maxima of the wave packet at the outer turning point are phase shifted by half a period with respect to the maxima at the inner turning point. Photoelectron spectra for $\lambda_2 = 265$ nm, 40 fs FWHM ionization are modeled either by discretization of the Na_2 electronic continuum based on techniques described in [28] or by a perturbative description [18].

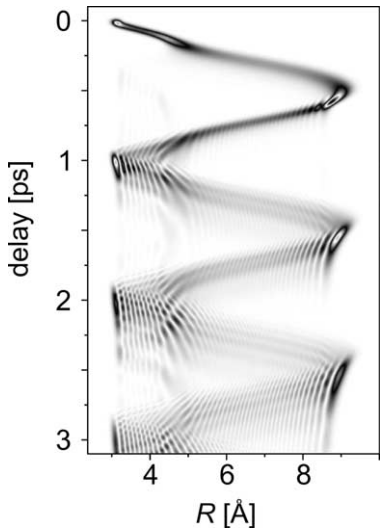

Fig. 2. Grey scale representation of the temporal evolution of the wave packet on the $2^1\Sigma_u^+$ double-minimum potential for $\lambda_1 = 340$ nm excitation. The wave packet is created at the equilibrium internuclear distance of the $X^1\Sigma_g^+$ ($v'' = 0$) ground state (3.1 Å) energetically above the barrier.

First we assume an R-independent transition dipole-moment for a neutral-to-ionic transition of equal magnitude for both ionic states. By variation of the R-dependence and comparison with the measured photoelectron spectra (Fig. 3a) the R-dependent ionization probability is extracted.

3. Experiment

We performed a two-color $\lambda_1 = 340$ nm pump and $\lambda_2 = 265$ nm ionization probe experiment on a Na_2 molecular beam with energy-resolved photoelectron detection. Na was heated to 870 K in an oven and expanded through a 100 μm nozzle seeded with Ar (1.6 bar) into a high vacuum chamber to produce a vibrationally cold Na_2 molecular beam. The 340 nm, 0.6 μJ and 5.5 nm FWHM pump pulses were generated by parametric amplification of 2/3 of the energy of the 1 kHz, 785 nm and 800 μJ output of a CPA Ti:Sapphire laser system and subsequent frequency quadrupling. Frequency tripling of the residual light of the amplifier provided the 265 nm, 0.4 μJ and 3.8 nm FWHM probe pulses. Both light pulses were polarized collinear to the axis of the time-of-flight (TOF) spectrometer. Optimizing the cross correlation of the Xe atom ionization signal with the help of prism compressors for the 340 and 265 nm pulses, the shortest pulses were obtained. The delay between the pump and probe laser pulses was set by a stepper motor driven delay line in a range of several picoseconds in 30 fs steps. With a $f = 250$ mm lens both laser beams were focussed to intersect the molecular beam. Photoelectrons from the interaction region were detected with a magnetic bottle TOF spectrometer with a resolution of 25 meV at 1 eV and 200 meV at 3 eV at the same settings. For each pump–probe delay photoelectron spectra were obtained by averaging over several thousand laser pulses. The kinetic energy calibration was performed with the lines of Na atoms also present in the molecular beam and photoelectrons from ionization of Xe atoms with the 355 nm radiation of a YAG laser. The stationary one-color signals from the atomic Na near resonance transition (3s–4p) at 2.2 eV (2×340 nm) and (3s–6p) at 4.2 eV (2×265 nm) and the two-color signal at 3.2 eV ($340 + 265$ nm) were subtracted from the measured photoelectron distribution and additional Gaussian averaging was applied.

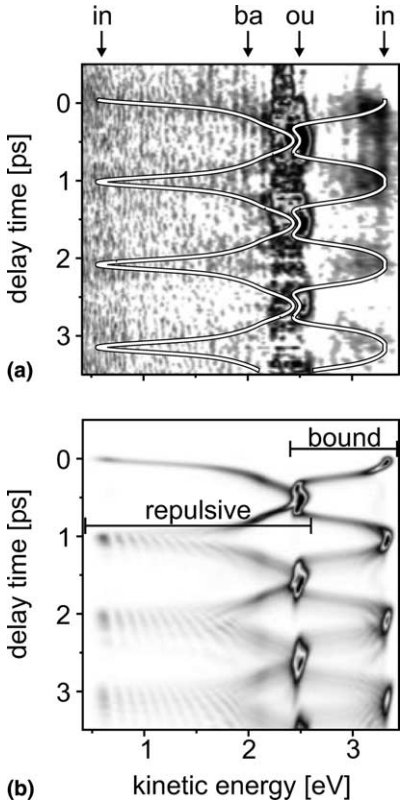

Fig. 3. (a) Measured and (b) calculated time evolution of the photoelectron spectra for $\lambda_1 = 340$ nm excitation and $\lambda_2 = 265$ nm ionization. The kinetic energy for inner (in) and outer (ou) turning point and the barrier (ba) is indicated with arrows. Photoelectrons from the repulsive and bound ionic state are observed at 0.4–2.6 and 2.4–3.5 eV, respectively (indicated with horizontal bars). Electrons from both ionic states formed at the outer turning point overlap at 2.5 eV. To guide the eye the measured signal is superimposed by the photoelectron energies obtained by classical trajectory calculation and difference potential analysis (white line in (a)).

4. Results

Fig. 3a shows a grey scale representation of the measured photoelectron spectra obtained within the first 3.5 ps time delay between pump and probe pulses. To enhance the visibility of the measured

signal the kinetic energy for 'classical electrons' is superimposed as a white line in Fig. 3a. For this purpose, classical trajectory calculations were performed to model the wave packet motion and the corresponding photoelectron energies were obtained from difference potential analysis [22]. For comparison the quantum-mechanically calculated photoelectron distributions from both the bound $1^2\Sigma_g^+$ ionic and the repulsive $1^2\Sigma_u^+$ ionic states are depicted (Fig. 3b). In the calculation the experimentally determined $\mu(R)$ was employed (see Section 5). Note that the electrons from both ionic curves overlap at a kinetic energy of 2.5 eV. Photoelectrons from the repulsive (bound) ionic state appear in the energy interval 0.4–2.6 eV (2.4–3.5 eV). At zero delay time between pump and probe pulses electrons are generated at the inner turning point corresponding to the ground state equilibrium position with a kinetic energy of 0.4 and 3.5 eV for the repulsive and bound ionic state, respectively. As the wave packet reaches the barrier it is dynamically enhanced which is seen around 2 eV on the repulsive state. Since the difference potential for the bound ionic state is almost flat between 3 and 4.5 Å (see dotted line in Fig. 1) all electrons within this interval are mapped onto a kinetic energy of about 3.5 eV. Therefore this dynamical effect is not seen in the bound branch. At 500 fs, when the wave packet arrives at the outer turning point, the kinetic energies of the photoelectrons from both ionic states coincide at 2.5 eV. The structured shape of the observed photoelectron distribution (cf. Figs. 3a and b at 2.5 eV, 500 fs) is due to this overlap and the non-monotonous relation of internuclear distance and kinetic energy on the bound ionic state around the outer turning point (see dotted line in Fig. 1 at 8 Å). The oscillations are repeatedly observed with a period of 1 ps. Note that the dynamic compression of the wave packet at the barrier at 2 eV recurs twice per period. To illustrate the phase shift between electrons from the outer turning point, the inner turning point and the barrier, sections along the pump–probe delay axis were taken at the respective kinetic energies of the measured and calculated photoelectron distributions as shown in Fig. 4. The calculated profiles were normalized to the peak height of the measured profiles. Measured and calculated profiles are in excellent agreement for the electrons generated at the outer turning point (Fig. 4a). Here the signal-to-noise ratio is best due to the localization of the packet (Fig. 2) and due to the overlapping kinetic energy windows of bound and repulsive ionic states (compare Fig. 3b). Even when the measured signal is close to the noise limit as for the photoelectrons from the repulsive ionic state at the inner turning point (Fig. 4c) the measured and calculated signals agree reasonably well. The phase of the photoelectrons from the outer turning point (Fig. 4a) and the inner turning point (Fig. 4b and c) are clearly shifted by half a period. Therefore the ionization pathway – i.e., whether the electrons are ionized at the inner or outer turning point – can be

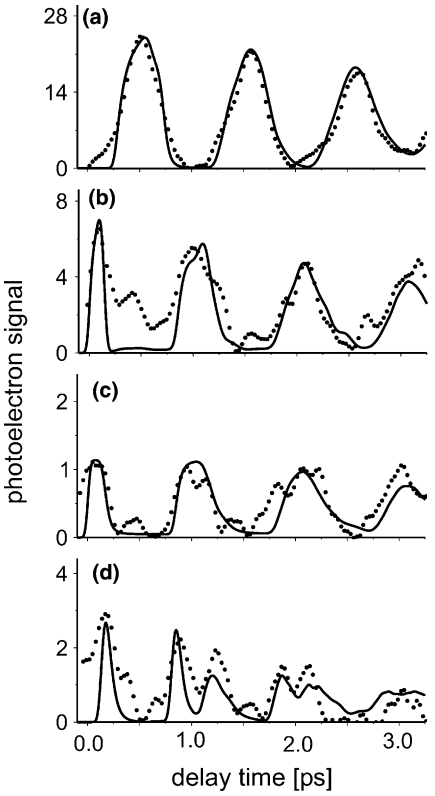

Fig. 4. Measured (dots) and calculated (lines) profiles of the photoelectrons from the outer turning point (repulsive and bound ionic potential) at 2.4–2.6 eV (a), the inner turning point (bound ionic potential) at 3.2–3.4 eV (b), the inner turning point (repulsive ionic potential) at 0.4–1.5 eV (c) and the barrier (repulsive ionic potential) at 1.8–2.2 eV (d).

unambiguously identified. Moreover the agreement with the calculation confirms that no measurable contributions from competing ionization channels are present. In the region of the barrier the photoelectrons monitor the twofold recurrence of the wave packet leading to an oscillation at twice the oscillation frequency as seen in Fig. 4d.

5. Discussion

Before we discuss the change of the transition dipole-moment for a neutral-to-ionic transition along the internuclear coordinate we consider possible additional ionization channels such as (i) energetically allowed high lying ionic states, (ii) photoelectrons from the C $2^1\Pi_u$ state and (iii) doubly excited autoionizing neutral states. (i) Besides the $1^2\Sigma_g^+$ and $1^2\Sigma_u^+$ ionic states the $2^2\Sigma_g^+$, $2^2\Sigma_u^+$ and the $1^2\Pi_g^+$, $1^2\Pi_u^+$ ionic states are also energetically accessible for 340 nm excitation and 265 nm ionization [29]. However, our analysis of the ionization probability is not affected for two reasons: first in the perturbative limit no population is lost from the initial (double-minimum) state in the presence of other target states, i.e., $\mu(R)$ is not underestimated through losses into competing channels. Second the difference potential analysis for all ionic states shows that photoelectrons from the other states should appear at low kinetic energy (below 0.75 eV) and would be generated predominantly at the outer turning point and therefore shifted by half a period with respect to the observed electrons from the repulsive $1^2\Sigma_u^+$ state. As no significant photoelectron signal is observed at low kinetic energy when the wave packet is located at the outer turning point (cf. minima at 500, 1500 fs, etc. in Fig. 4c) we can exclude an overestimation of $\mu(R)$ through photoelectrons from other ionization pathways. (ii) At 340 nm the Na_2 $2^1\Pi_u$ (C) state could also be excited [26]. The difference potential analysis for the C state predicts photoelectrons around 1 eV with an oscillation period corresponding to a vibrational level spacing of 114 cm^{-1} from the $1^2\Sigma_u^+$ ionic state and stationary photoelectrons from the $1^2\Sigma_g^+$ ionic state around 3.5 eV which are both not seen in our experiment (Fig. 3a). From the high lying ionic states only the $1^2\Pi_u^+$ state could contribute photoelectrons at 0.5 eV with an oscillation period of 114 cm^{-1} which are also not observed. Therefore the $2^1\Pi_u$ (C) state does not contribute significantly in our experiment. (iii) For autoionizing doubly excited states a lifetime of at least half the vibrational period has been reported [30]. This leads to a broad photoelectron distribution. Accordingly stripes in the photoelectron spectrum should be visible at the corresponding Franck–Condon-windows due to the localized excitation into these states. However, no such stripes are observed in the experiment. Therefore these additional channels are ruled out. In order to evaluate the $\mu(R)$ dependence, measured and calculated photoelectron spectra were averaged over one oscillation period (533–1533 fs). The choice of the time window introduces less than 10% variation of the ratio of integrated photoelectrons within the energy intervals of the two pronounced peaks at 2.1–2.7 eV (outer turning point) and 2.8–3.5 eV (inner turning point, bound ionic potential). This analysis was used to determine the experimental error. In Fig. 5 the measured average is compared to calculated spectra averaged over the same interval of delays. The calculated spectra are convoluted with a resolution of 0.2 eV. Generally, the transition dipole-moment for a neutral-to-ionic transition could be a discontinuous function of the internuclear separation for both ionic states. In this case the individual dipole moments cannot be extracted for the internuclear distances which are mapped onto identical kinetic energies. This is a general problem at large internuclear distances when the *gerade* and *ungerade* ionic potentials converge. Therefore we proceed in three steps: we start by assuming a R-independent dipole moment of equal magnitude for both ionic states. Then the R-independent dipole moment for the repulsive ionic state is adjusted and finally a linear variation of the dipole moment for the bound ionic state $\mu_b(R)$ is considered. Fig. 5a shows the averaged spectrum for R-independent dipole moments of equal magnitude for both ionic states, i.e., $\mu_r = \mu_b = \mu_0$. The value of μ_0 was adjusted to fit the photoelectrons from the bound ionic state at 3.3 eV. Obviously, the photoelectrons from the repulsive ionic state at the barrier around 2 eV are

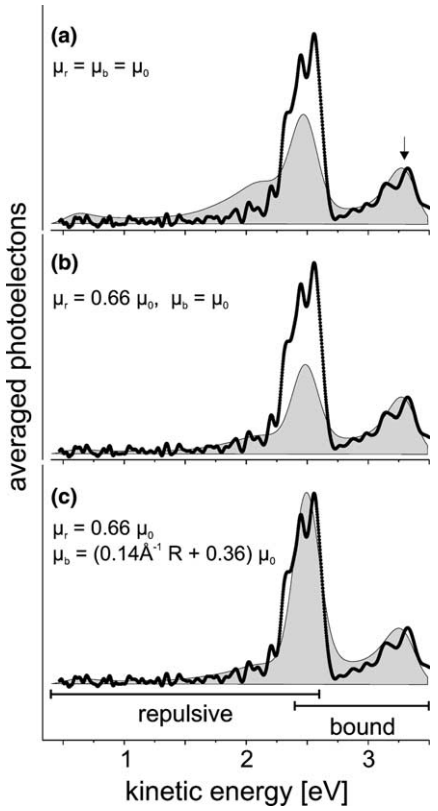

Fig. 5. Measured (bold) and calculated (light grey) photoelectron spectra averaged over one oscillation period (533–1533 fs). Calculated spectra for constant transition dipole-moment for a neutral-to-ionic transition with (a) $\mu_r = \mu_b = \mu_0$ and (b) reduced $\mu_r = 0.66\mu_0$ and (c) assuming a constant dipole moment for the repulsive state ($\mu_r = 0.66\mu_0$) and a linearly increasing dipole moment for the bound state $\mu_b = (0.14\ \text{Å}^{-1}R + 0.36)\mu_0$.

overestimated in the calculation and the photoelectrons at 2.5 eV are clearly underestimated in the calculation. Because the signal-to-noise ratio at low kinetic energies (0.4 – 1.0 eV) does not allow to quantitatively analyze the R-dependence of the transition dipole-moment for a neutral-to-ionic transition to the repulsive ionic state we assume an R-independent μ_r as a zeroth-order approximation. In Fig. 5b μ_r is reduced to $0.66\mu_0$ to match the measurement at the barrier. In order to reproduce the measured spectrum in the overlapping region at 2.5 eV as well, a linear increasing dipole moment for ionization into the bound state is assumed. A good agreement of measured and calculated averaged photoelectron spectra is obtained for $\mu_b = (0.14\ \text{Å}^{-1}R + 0.36)\mu_0$ as shown in Fig. 5c. Since the ionization probability is proportional to the square of the dipole moment we find that for the bound ionic state the ionization probability at the outer turning point is $(\mu_b\ (8.8\ \text{Å})/\mu_b\ (3.1\ \text{Å}))^2 = 4.0 \pm 0.4$ times the ionization probability at the inner turning point. Moreover, at the outer turning point the ionization probability for the bound state is roughly $(\mu_b\ (8.8\ \text{Å})/\mu_r\ (8.8\ \text{Å}))^2 = 6.0 \pm 0.6$ times larger than the ionization probability for the repulsive state.

6. Conclusion

With the help of energy-resolved photoelectron detection an unambiguous identification of the ionization pathway was achieved in our experiment. First, a clear distinction between ionization at the inner and outer well from the Na_2 double-minimum state and the corresponding photoelectrons from both the bound and repulsive ionic state was made. Second, competing processes such as contributions from other high lying ionic states or doubly excited autoionizing neutral states were ruled out and no signal from the energetically close lying C $2^1\Pi_u$ state was observed. The variation of $\mu(R)$ is observed such that (i) ionization to the bound ionic state is favored at all internuclear distances and (ii) for the bound ionic state the ionization probability at the outer turning point is 4.0 ± 0.4 times larger than at the inner turning point. Our results demonstrate the utilization of wave packets as a local probe for an R-dependent ionization probability and in particular the usefulness of energy-resolved photoelectron detection to unambiguously identify the ionization pathway. To further exploit the potential of this technique on the Na_2 double-minimum state a systematic study of pump–probe photoelectron spectra for a range of (i) pump and (ii) probe wavelengths is planned in our laboratory. This will allow to (i) separately study interference effects in the wave packet dynamics at the barrier and also (ii) to investigate the R-dependent photoionization probability in the high and low kinetic energy limit.

Acknowledgements

Support of the Deutsche Forschungsgemeinschaft, the Fonds der Chemischen Industrie and the NRC-Helmholtz program is gratefully acknowledged.

References

[1] P. Cong, G. Roberts, J.L. Herek, A. Mohktari, A.H. Zewail, J. Phys. Chem. 100 (1996) 7832.
[2] L. Pesce, Z. Amitay, R. Uberna, S.R. Leone, M. Ratner, R. Kosloff, J. Chem. Phys. 114 (2001) 1259.
[3] V. Blanchet, M.Z. Zgierski, A. Stolow, J. Chem. Phys. 114 (2001) 1194.
[4] M. Wollenhaupt, A. Assion, O. Bazhan, D. Liese, C. Sarpe-Tudoran, T. Baumert, Appl. Phys. B 74 (2002) S121.
[5] C. Jouvet, S. Martrenchard, D. Solgadi, C. Dedonder-Lardeux, M. Mons, G. Grégoire, I. Dimicoli, F. Piuzzi, J.P. Visticot, J.M. Mestdagh, P. D'Oliveira, P. Meynadier, M. Perdrix, J. Phys. Chem. A 101 (1997) 2555.
[6] G. Grégoire, M. Mons, I. Dimicoli, F. Piuzzi, E. Charron, C. Dedonder-Lardeux, C. Jouvet, S. Martrenchard, D. Solgadi, A. Suzor-Weiner, Eur. Phys. J. D 1 (1998) 187.
[7] H. Schwoerer, R. Pausch, M. Held, V. Engel, W. Kiefer, J. Chem. Phys. 107 (1997) 9749.
[8] C. Nicole, M.A. Bouchène, C. Meier, S. Magnier, E. Schreiber, B. Girard, J. Chem. Phys. 111 (1999) 7857.
[9] R. Andersson, M. Kadi, J. Davidsson, T. Hansson, Chem. Phys. Lett. 352 (2002) 106.
[10] A. Valance, Q. Nguyen Tuan, J. Phys. B 15 (1982) 17.
[11] W. Domcke, G. Stock, Adv. Chem. Phys. 100 (1997) 1.
[12] Y. Arasaki, K. Takatsuka, K. Wang, V. McKoy, Chem. Phys. Lett. 302 (1999) 363.
[13] Y. Arasaki, K. Takatsuka, K. Wang, V. McKoy, J. Chem. Phys. 112 (2000) 8871.
[14] Y. Arasaki, K. Takatsuka, K. Wang, V. McKoy, J. Chem. Phys. 114 (2001) 7941.
[15] K. Takatsuka, Y. Arasaki, K. Wang, V. McKoy, Faraday Discuss. 115 (2000) 1.
[16] A. Assion, T. Baumert, V. Seyfried, V. Weiss, E. Wiedenmann, G. Gerber, Z. Phys. D 36 (1996) 265.
[17] A. Assion, T. Baumert, M. Geisler, V. Seyfried, G. Gerber, Eur. Phys. J. D 4 (1998) 145.
[18] C. Meier, V. Engel, J. Chem. Phys. 101 (1994) 2673.
[19] S. Meyer, C. Meier, V. Engel, J. Chem. Phys. 108 (1998) 7631.
[20] T. Lohmüller, M. Erdmann, V. Engel, Chem. Phys. Lett. 373 (2003) 319.
[21] T. Baumert, B. Buehler, R. Thalweiser, G. Gerber, Phys. Rev. Lett. 64 (1990) 733.
[22] A. Assion, M. Geisler, J. Helbing, V. Seyfried, T. Baumert, Phys. Rev. A 54 (1996) R4605.
[23] T. Seideman, Annu. Rev. Phys. Chem. 53 (2002) 41.
[24] T. Suzuki, B.J. Whitaker, Int. Rev. Phys. Chem. 20 (2001) 313.
[25] J.A. Davies, R.E. Continetti, D.W. Chandler, C.C. Hayden, Phys. Rev. Lett. 84 (2000) 5983.
[26] R. Haugstätter, A. Goerke, I.V. Hertel, Z. Phys. D 9 (1998) 153.
[27] F. Großmann, J.M. Rost, W.P. Schleich, J. Phys. A 30 (1997) L277.
[28] E. Charron, A. Suzor-Weiner, J. Chem. Phys. 108 (1998) 3922.
[29] A. Assion, T. Baumert, U. Weichmann, G. Gerber, Phys. Rev. Lett. 86 (2001) 5695.
[30] T. Baumert, M. Grosser, R. Thalweiser, G. Gerber, Phys. Rev. Lett. 67 (1991) 3753.